Wax-printing-free fabrication of paper-supported 3D cancer cell culture

Ankit Kumar[1], Shweta Kumar[1], Bhushan J. Toley[1,2*]

[1]Department of Chemical Engineering
Indian Institute of Science
Bangalore, Karnataka, 560012

[2]Department of Bioengineering
Indian Institute of Science
Bengaluru, Karnataka 560012
India

Keywords: tumor microenvironment, hypoxia, doxorubicin, drug diffusion, drug screening

*Correspondence to:
Bhushan J. Toley
Department of Chemical Engineering
Indian Institute of Science, Bangalore
Malleswaram
Bangalore 560012
Phone: +91-9146142296
Email: bhushan@iisc.ac.in

S1: Literature review

Table S1: Compilation of reports of paper-based tissue engineering

Study	Cell Type	Platform	Layers	Application	Analysis Method	Patterning / Assembly	Ref.
Derda et al., 2009	MDA-MB-231, HS-5	Paper-supported 3D cell culture	1–8	Tumor model, oxygen/nutrient gradients	Viability, gene expression	No wax barriers; stacked filter paper	[1]
Mosadegh et al., 2015	Cardiomyocytes	CiGiP ischemia model	3–8	Cardiac ischemia	Immunostaining, viability	Wax-patterned paper	[2]
Kenney et al., 2015	MDA-MB-231	Multilayer paper culture	6–10	Oxygen gradient analysis	Luminescent oxygen films	PDMS tape assembly	[3]
Chung et al., 2018	N/A	Paper-based gradient model	10	pH gradient visualization	pH-sensitive films	Adhesive lamination	[4]
Deiss et al., 2013	MDA-MB-231	High-throughput CiGiP platform	3	Drug screening	Gel scanner, ImageJ	Wax-patterned paper with PDMS gasket	[5]
Deiss et al., 2014	MDA-MB-231	Peptide-functionalized paper scaffold	1	Cell adhesion studies	Fluorescence imaging	Teflon-patterned paper	[6]
Rodenhizer et al.	Cancer cells	TRACER platform	6	Oxygen/nutrient gradients	Fluorescence imaging	Rolled tissue architecture	[7]
Sapp et al., 2015	Aortic valvular interstitial cells	Multilayer collagen-paper construct	3–7	Cell migration, hypoxia response	Confocal microscopy, gel scanner	Wax-patterned filter paper	[8]
Rahimi et al., 2016	CALU-3	Respiratory tissue model	Single membrane	Air-liquid interface culture	Live/Dead, ZO-1 staining	Laser-patterned parchment paper	[9]
Hong et al., 2016	HeLa	Paper-based gradient generator	Single layer	Drug screening	Calcein/PI, PrestoBlue	SU-8 photolithography	[10]

Tao et al., 2015	Huh-7	Paper microfluidic culture platform	Single layer	Drug screening	WST-1 assay, SEM	Wax-patterned paper	[11]
Supjaroen et al., 2025	Caco-2	3D printed transwell-paper device	Single membrane	Intestinal barrier model	TEER, FITC permeability, IF	Wax-patterned paper	[12]
Sitte et al., 2024	MDA-MB-231, HUVEC, RMF	Perfused scaffold culture system	Multiple scaffold layers	Perfusion culture, vascular model	Live/Dead, permeability assay	Wax-patterned scaffold + 3D printed perfusion device	[13]

S2. Design of the 3D-printed stacked paper tissue device

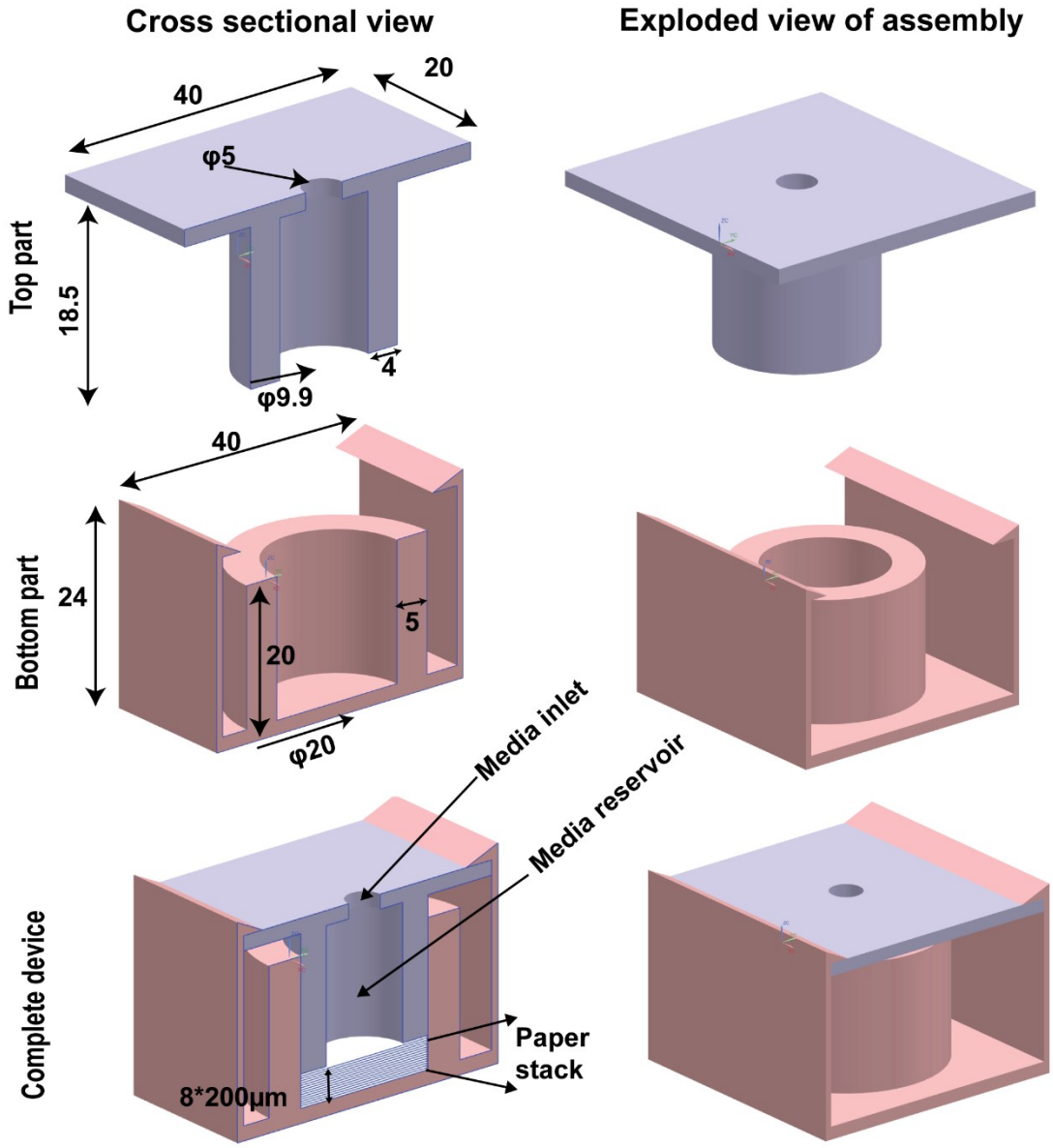

Figure S2: Design of the 3D-printed stacked-paper tissue culture device. All dimensions are in units of mm unless otherwise specified.

S3. Culture of MDA-MB-231 cells on different paper-based substrates in Matrigel

MDA-MB-231 cells, a model for aggressive breast cancer, are cultured on various substrates to study their growth and behaviour. The percentage of live and dead cells was calculated as:

$$\%\ Live\ Cells = \frac{Number\ of\ live\ cells}{Number\ of\ live\ cells + Number\ of\ dead\ cells} \times 100$$

$$\%\ Dead\ Cells = \frac{Number\ of\ dead\ cells}{Number\ of\ live\ cells + Number\ of\ dead\ cells} \times 100$$

No significant difference in cell proliferation was observed across the membranes. Whatman filter paper 1 was chosen as the membrane to proceed with because of its mechanical stability during destacking and the clarity of fluorescent images generated.

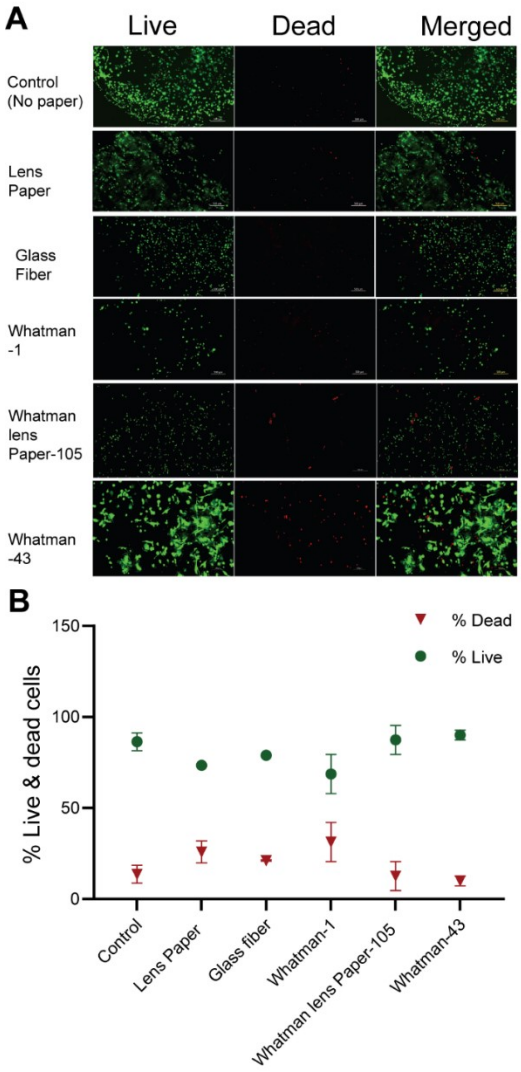

Figure S3:(A) Live and dead cell-stained image of MDA-MB-231 cells grown in Matrigel (10x magnification). The scale bar in the image is 200 μm (B). Plot of percentage live and dead cells in different papers.

S4. Assessment of platform performance using Whatman lens paper-105

To further assess the applicability of the device to thin and mechanically less robust paper substrates, an additional experiment was performed using Whatman lens paper-105 with an approximate thickness of 40 μm. Cells were seeded onto a single paper layer and cultured for 48 h prior to device assembly. This pre-seeded layer was positioned at L-5 in the stacked device, while all other layers were kept cell-free at the time of stacking. The assembled device was then further incubated until a total culture time of 72 h. After incubation, the individual layers were separated and imaged by fluorescence microscopy for live-cell observation. Cell distribution across the layers was assessed by measuring fluorescence intensity from the acquired images. The imaging procedure was the same as that described in the main manuscript.

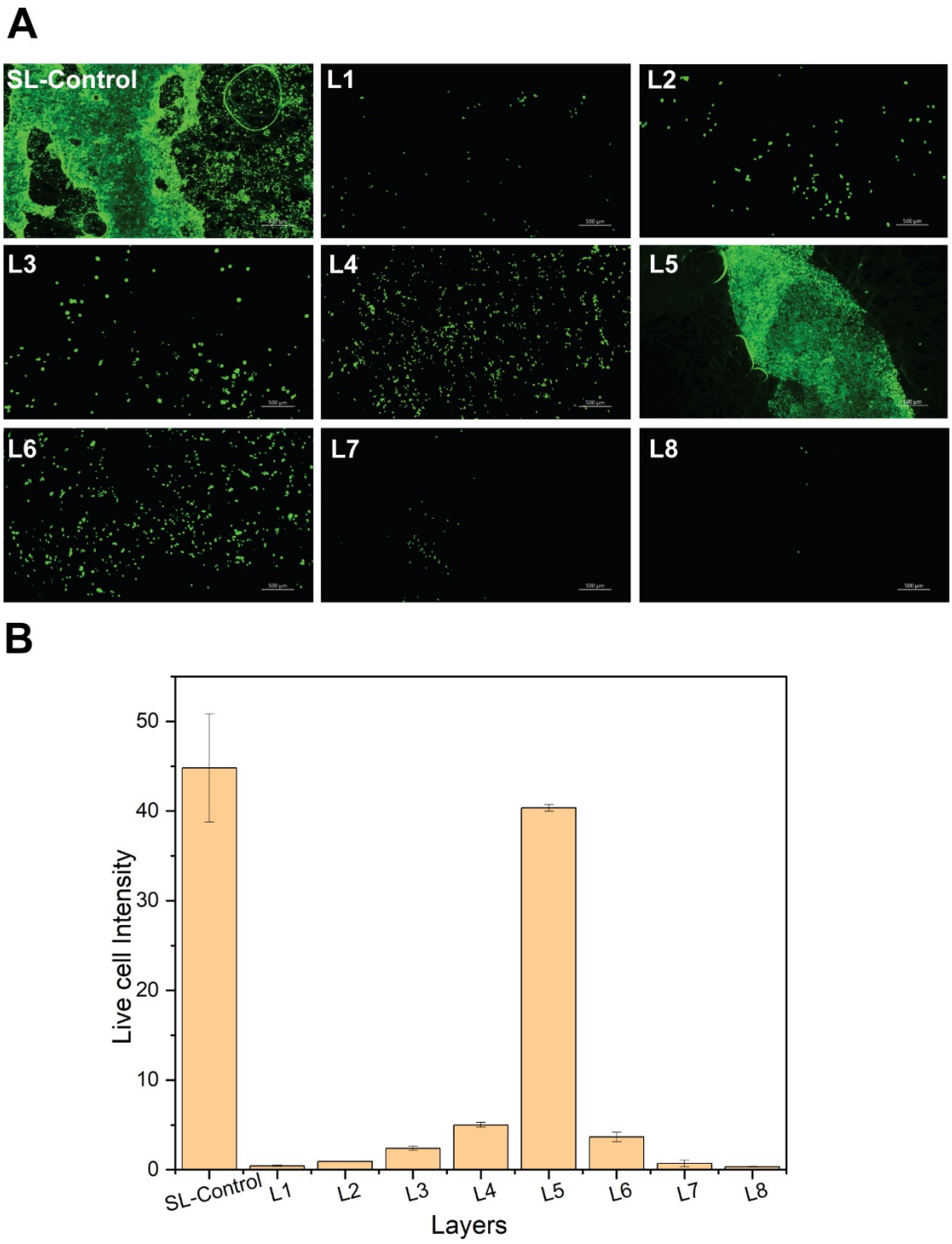

Figure S4: Evaluation of cell migration across stacked layers using thin Whatman lens paper-105.**(A)** Representative fluorescence microscopy images of live cells in the separated paper layers after 72 h of culture. Cells were pre-cultured for 48 h on a single Whatman lens paper-105 layer and this cell-seeded layer was placed at L-5 during device assembly. All remaining layers were cell-free at the time of stacking. After further incubation to 72 h, cells were observed in L-2 and L-7, indicating migration from the initially seeded L-5 layer. **(B)** Quantification of fluorescence intensity across the layers after 72 h, obtained from live-cell fluorescence microscopy images.

To further assess the applicability of the platform to thin and mechanically less robust paper substrates, additional experiments were performed using Whatman lens paper-105. When only the L-5 layer was pre-seeded with cells, and all other layers were cell-free at the time of stacking, cells were subsequently detected in L-2 and L-7 after 72 h, confirming migration from the initially seeded layer (Figure S4).

S5. Growth and behaviour of MDA-MB-231 cells on various substrates involving collagen and Matrigel

MDA-MB-231 cells were grown under 4 conditions – i) in collagen without paper, ii) in paper without collagen, iii) in collagen in paper, and iv) in Matrigel in paper. Percentage live cells after a growth period of 48 hours is shown in Figure S5. There was no significant difference between conditions iii) and iv), and cells in Matrigel in paper was chosen as the matrix of choice for its physiological relevance as well as its ability to gel rapidly after introduction into paper.

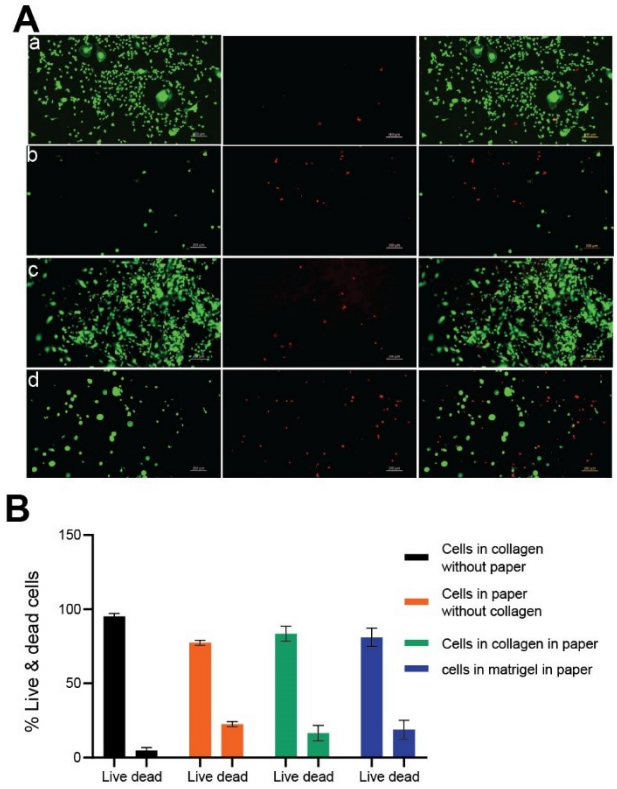

Figure S5:(A) Live and dead cell-stained image of MDA-MB-231 cells grown in (a) Cells in gel without paper, (b) Cells in paper without gel, (c) Cells in collagen in paper, (d) Cells in Matrigel in paper at 10x magnification. The scale bar of the image is 200 µm. (B) Plot of percentage live and dead cells in various substrates**.**

MDA-MB-231 cells exhibited high viability under all gel-supported culture conditions, indicating that both collagen and Matrigel provided a favorable microenvironment for cell survival. In contrast, cells cultured in paper without an extracellular matrix exhibited lower viability and reduced cell density, highlighting the importance of a supporting matrix for cell attachment and growth. No significant difference in viability was observed between collagen-

in-paper and Matrigel-in-paper conditions, demonstrating that both matrices effectively supported cell survival within the paper scaffold. Matrigel was selected for subsequent experiments because of its physiological relevance, rapid gelation characteristics, and ease of incorporation into the paper substrate. These results confirm that the paper scaffold is compatible with hydrogel-supported cell culture and can maintain high cell viability over the experimental period.

S6. Kinetic study of MDA-MB-231 cells growing in Matrigel in Whatman filter paper Grade-1

To assess whether MDA-MB-231 cells were proliferating, 0.1 million cells/mL were seeded in Matrigel in Whatman filter paper (Grade 1) placed in 12-well plates. The cells were incubated in an environment consisting of 5% CO_2, 37 °C, and 15% humidity for 0, 24, 48, 72, and 120 hours. After each incubation period, the cells were stained with Calcein-AM to label live cells (green fluorescent). The acquired image shows live cells (Figure S6A), and the acquired images were imported into ImageJ and converted to an 8-bit grayscale format. The average pixel intensity was quantified for each image frame using ImageJ for per field of view (FOV) . Intensity measurements were performed for three independent experiments, and the mean values were calculated, as depicted in Figure S6B.

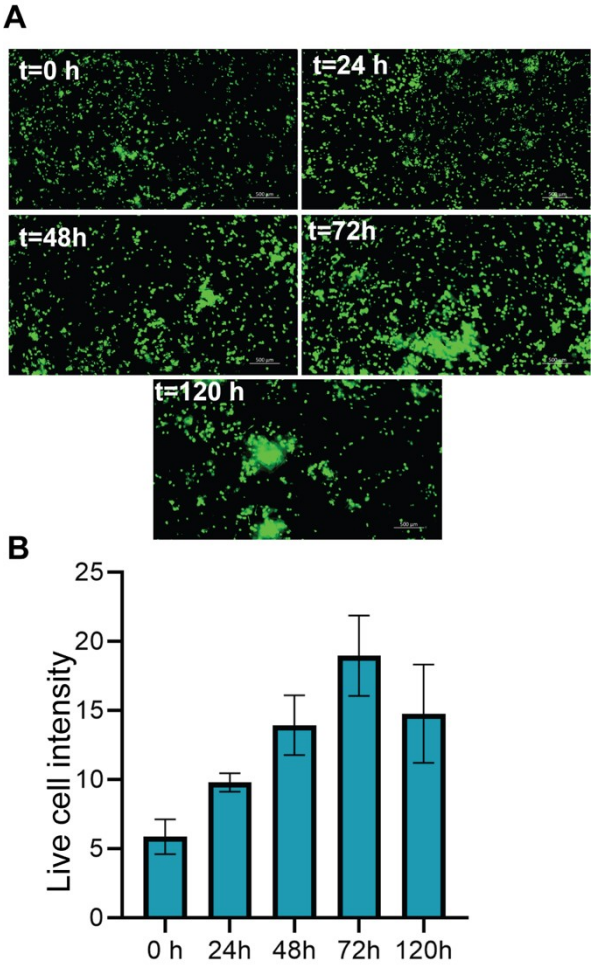

Figure S6: (A) Fluorescent image of live(green) MDA-MB-231 cells in Matrigel after staining with Calcein-AM at various times. The scale bar of the image is 200 μm. (B) Plot of live cell intensity at different times.

Figure S6 demonstrates the ability of the paper scaffold to support long-term growth of MDA-MB-231 cells. Live-cell intensity increased progressively from 0 to 72 h, indicating successful cell attachment and proliferation. Following medium replacement at 48 h, continued cell growth was observed, with the highest live-cell intensity recorded at 72 h. At 120 h, a reduction in average live-cell intensity was observed. Visual inspection of the fluorescence images suggests the formation of larger cellular aggregates at later time points, indicating changes in cellular organization during prolonged culture. The reduction in signal may therefore result

from a combination of cellular clustering, local nutrient/metabolite gradients within the scaffold, and gradual loss of viability in a subset of cells. These findings demonstrate that the paper scaffold supports sustained cell growth and viability for at least 72 h.

S7. Transport of FITC-dextran of different molecular weights in the 3D paper stack

To investigate the diffusion of molecules with varying molecular weights through stacked paper layers, eight PBS-saturated paper layers were assembled within a 3D-printed device. FITC-dextran – 4 kDa and 40 kDa – was then introduced at concentrations of 100 µM into the top culture chamber. After 1 hour, the layers were de-stacked, and fluorescence images of each layer were captured using a fluorescent microscope. The experiments were performed in triplicate, and the mean and standard deviation of fluorescence intensity were plotted for each layer for both molecules. The intensity of both molecules was similar in L1 and decreased with increasing layer number, but decreased more rapidly for FITC-dextran 40 kDa compared to FITC-dextran 4 kDa (Fig. S7 A-B). This demonstrates the tissue model's ability to accurately reproduce transport limitations faced by molecules of different molecular weights.

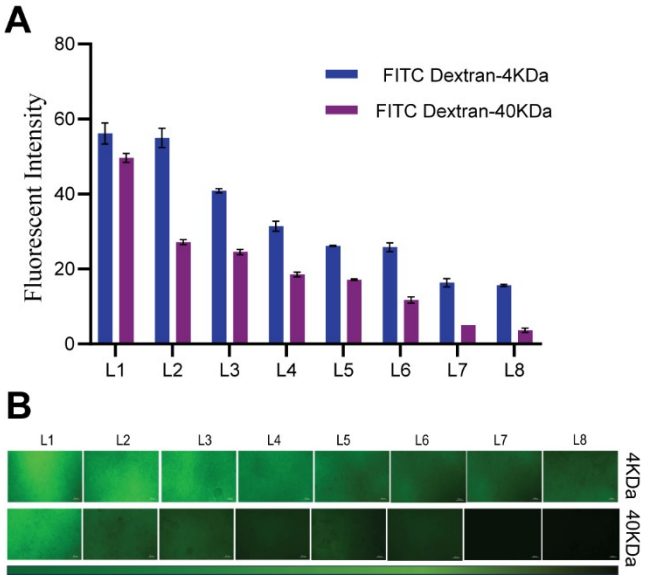

Figure S7: (A) Fluorescence intensity profiles of FITC–dextran (4 kDa) and FITC–dextran (40 kDa) across stacked layers of Whatman filter paper grade 1 after 1 h of treatment. (B) Fluorescence images of FITC–dextran (4 and 40 kDa) across stacked layers. The scale bar of the image is 200 μm.

S8. Pharmacodynamic Analysis of Doxorubicin, Paclitaxel, and their Combination in a Single Layer (SL) Cell Culture.

Cells were seeded at a density of 0.1 million cells/mL in Matrigel in paper, which was then placed in 12-well plates. The cultures were incubated for 48 hours under standard conditions (37 °C, 5% CO_2, and a humidified atmosphere) in drug-free medium to allow for equilibration. The medium was then removed, and the cells were washed with PBS. Cells were subsequently treated with doxorubicin (DOX), paclitaxel (PTX), and a combination of DOX and PTX at concentrations of 0.1, 1, 10, 25, and 50 μM. After 72 h of drug exposure, the drug-containing medium was removed, cells were washed with PBS, and cell viability was assessed by staining with calcein-AM. Live-cell imaging was performed using fluorescence microscopy in the FITC channel at 10× magnification. The acquired images were imported into the ImageJ software for quantification of live-cell fluorescence intensity. Images were converted to 8-bit grayscale format, and the average fluorescence intensity per field of view(FOV) was calculated for each image. This analysis was performed for all images and repeated across three independent experimental samples.

In Figure S8A, it can be clearly observed that the intensity of live cells decreases as the drug concentration increases. This indicates a strong pharmacodynamic effect of the drug, both for the individual treatments and their combination. From these intensity values, percent cell viability was calculated and plotted to show the viability across different concentrations of

doxorubicin, paclitaxel, and their combination. Percentage inhibition was calculated as 100 minus the percentage cell viability.

$$\%\ Cell\ Viability = \frac{Live\ cells\ intensity(c)}{Live\ cell\ intensity(c = 0\mu M)}$$

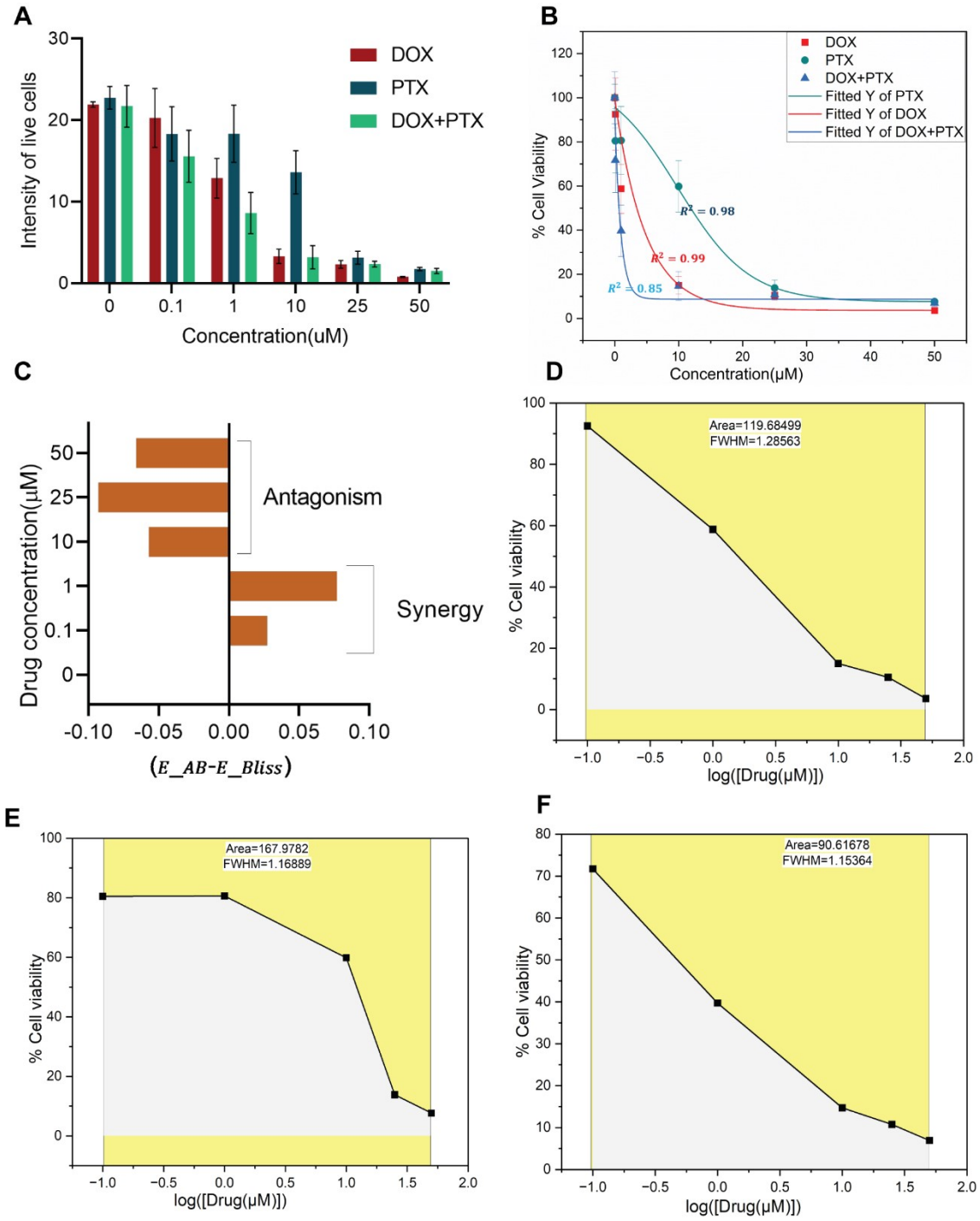

Figure S8: (A) Live-Cell Fluorescence Intensity of Cells Treated with DOX, PTX, and DOX+PTX at Varying Concentrations. (B) Dose-Dependent Cell Viability Following DOX,

PTX, and DOX+PTX Treatment. (C) BLISS Score Analysis of DOX–PTX Combination Across Drug Concentrations. (D–F) Dose–response curves showing percentage cell viability as a function of log(drug concentration) for DOX (D), PTX (E), and DOX+PTX (F).

Next, we fitted the experimentally obtained percentage viability data to a pharmacodynamic dose–response model (equation S1) to determine the IC_{50} value—a well-known parameter that reflects the potency of a drug (Figure S8B). The combination treatment exhibited a lower IC_{50} value compared to the individual drugs, indicating greater potency in the combined formulation (Table S2). It is important to clarify that the dose–response curves for doxorubicin (DOX) and paclitaxel (PTX) individually exhibited excellent fits to the sigmoidal model, with R^2values of 0.99 and 0.98, respectively. In contrast, the combination treatment yielded a lower R^2value of 0.85. We hypothesize that this reduction arises because the combination response does not follow a simple sigmoidal relationship across the entire concentration range. Specifically, synergistic effects were observed at lower concentrations, whereas antagonistic effects were observed at higher concentrations. Such concentration-dependent changes in drug interaction can cause deviations from a single sigmoidal dose–response profile, resulting in a poorer overall fit.

$$Y(\%\ Cell\ Viability) = A_1 + \frac{A_1 - A_2}{1 + 10^{\left(logIC_{50} - X\right) \times n}} \qquad (S1)$$

Table S2: IC_{50}(μM) for all drug treatments in a single layer(SL).

Drugs	**IC_{50}(μM)**
Doxorubicin(DOX)	2.24
Paclitaxel (PTX)	12.1
DOX+PTX	0.6

The BLISS score (methods described in the main text) was then calculated and is reported in Fig. S8C. The BLISS score analysis revealed concentration-dependent interactions between DOX and PTX. Positive BLISS scores were observed at lower drug concentrations (0.1–1 μM), indicating mild synergistic interactions. In contrast, negative BLISS scores were observed at higher concentrations (10–50 μM), suggesting antagonistic behavior. Overall, antagonism was the dominant interaction at moderate-to-high concentrations, whereas limited synergy was observed only within a narrow low-concentration range. Finally, the area under the curve (AUC) was determined for the dose–response curves of both individual and combination treatments to assess drug efficacy (Figures S8-D–F). The combination treatment exhibited a smaller AUC compared to the individual drugs, indicating enhanced potency and efficacy in the single-layer (SL) cell culture model.

References

(1) Derda, R.; Laromaine, A.; Mammoto, A.; Tang, S. K. Y.; Mammoto, T.; Ingber, D. E.; Whitesides, G. M. *Paper-Supported 3D Cell Culture for Tissue-Based Bioassays*. www.pnas.org/cgi/content/full/.

(2) Mosadegh, B.; Lockett, M. R.; Minn, K. T.; Simon, K. A.; Gilbert, K.; Hillier, S.; Newsome, D.; Li, H.; Hall, A. B.; Boucher, D. M.; Eustace, B. K.; Whitesides, G. M. A Paper-Based Invasion Assay: Assessing Chemotaxis of Cancer Cells in Gradients of Oxygen. *Biomaterials* **2015**, *52* (1), 262–271. https://doi.org/10.1016/j.biomaterials.2015.02.012.

(3) Kenney, R. M.; Loeser, A.; Whitman, N. A.; Lockett, M. R. Paper-Based Transwell Assays: An Inexpensive Alternative to Study Cellular Invasion. *Analyst* **2019**, *144* (1), 206–211. https://doi.org/10.1039/c8an01157e.

(4) Peng, C. C.; Liao, W. H.; Chen, Y. H.; Wu, C. Y.; Tung, Y. C. A Microfluidic Cell Culture Array with Various Oxygen Tensions. *Lab Chip* **2013**, *13* (16), 3239–3245. https://doi.org/10.1039/c3lc50388g.

(5) Deiss, F.; Mazzeo, A.; Hong, E.; Ingber, D. E.; Derda, R.; Whitesides, G. M. Platform for High-Throughput Testing of the Effect of Soluble Compounds on 3D Cell Cultures. *Anal. Chem.* **2013**, *85* (17), 8085–8094. https://doi.org/10.1021/ac400161j.

(6) Deiss, F.; Matochko, W. L.; Govindasamy, N.; Lin, E. Y.; Derda, R. Flow-through Synthesis on Teflon-Patterned Paper to Produce Peptide Arrays for Cell-Based Assays. *Angew. Chem. Int. Ed.* **2014**, *53* (25), 6374–6377. https://doi.org/10.1002/anie.201402037.

(7) Rodenhizer, D.; Cojocari, D.; Wouters, B. G.; McGuigan, A. P. Development of TRACER: Tissue Roll for Analysis of Cellular Environment and Response. *Biofabrication* **2016**, *8* (4). https://doi.org/10.1088/1758-5090/8/4/045008.

(8) Sapp, M. C.; Fares, H. J.; Estrada, A. C.; Grande-Allen, K. J. Multilayer Three-Dimensional Filter Paper Constructs for the Culture and Analysis of Aortic Valvular Interstitial Cells. *Acta Biomater.* **2015**, *13*, 199–206. https://doi.org/10.1016/j.actbio.2014.11.039.

(9) Rahimi, R.; Htwe, S. S.; Ochoa, M.; Donaldson, A.; Zieger, M.; Sood, R.; Tamayol, A.; Khademhosseini, A.; Ghaemmaghami, A. M.; Ziaie, B. A Paper-Based: In Vitro Model for on-Chip Investigation of the Human Respiratory System. *Lab Chip* **2016**, *16* (22), 4319–4325. https://doi.org/10.1039/c6lc00866f.

(10) Hong, B.; Xue, P.; Wu, Y.; Bao, J.; Chuah, Y. J.; Kang, Y. A Concentration Gradient Generator on a Paper-Based Microfluidic Chip Coupled with Cell Culture Microarray for High-Throughput Drug Screening. *Biomed. Microdevices* **2016**, *18* (1), 1–8. https://doi.org/10.1007/s10544-016-0054-2.

(11) Tao, F. F.; Xiao, X.; Lei, K. F.; Lee, I. C. Paper-Based Cell Culture Microfluidic System. *Biochip J.* **2015**, *9* (2), 97–104. https://doi.org/10.1007/s13206-015-9202-7.

(12) Supjaroen, P.; Niamsi, W.; Thummarati, P.; Laiwattanapaisal, W. An In Vitro Cell Model of Intestinal Barrier Function Using a Low-Cost 3D-Printed Transwell Device and Paper-Based Cell Membrane. *Int. J. Mol. Sci.* **2025**, *26* (6). https://doi.org/10.3390/ijms26062524.

(13) Sitte, Z. R.; Karlsson, E. E.; Li, H.; Zhou, H.; Lockett, M. R. Continuous Flow Delivery System for the Perfusion of Scaffold-Based 3D Cultures. *Lab Chip* **2024**, *24* (17), 4105–4114. https://doi.org/10.1039/d4lc00480a.